Neuroradiology (1987) 29: 238–245

Neuroradiology

STIR sequences in NMR imaging of the optic nerve

G. Johnson, D. H. Miller, D. MacManus, P. S. Tofts, D. Barnes, E. P. G. H. du Boulay, and W. I. McDonald

Institute of Neurology and National Hospitals for Nervous Diseases, Queen Square, London, UK

Summary. Orbital fat surrounding the optic nerve causes considerable difficulties in NMR imaging due to its high image intensity and the chemical shift artefact. We have investigated the ability of inversion recovery sequences with short inversion times (STIR sequences) to suppress fat signals in imaging the optic nerve. We have also compared the contrast attainable with STIR sequences with that obtainable from other sequences. Measurements were made on 4 normal controls and 5 patients with multiple sclerosis (MS) to obtain typical values of relaxation times and proton densities for orbital fat, cerebral white matter and MS lesions. The fat T_1 measurements were used to predict an appropriate inversion time for the STIR sequence and estimate how much residual fat signal might be expected as a result of natural variations in fat T_1. STIR sequences can be used to suppress the signal from orbital fat with little residual signal. Measurements from white matter and MS lesions were used to predict the contrast between normal and pathological tissues that is attainable with STIR sequences. STIR contrast compares favourably with that obtainable from other sequences.

Key words: NMR imaging – Optic nerve – Chemical shift artefact – Contrast

Imaging the optic nerve and its abnormalities has proved unsatisfactory although it is apparently so accesible. In research into multiple sclerosis (MS) the ability to visualise optic neuritis may be important and we have therefore attempted to improve our ability to image it.

The optic nerve and its sheath form an approximate cylinder 4–5 mm in diameter surrounded by orbital fat. The NMR signal from the optic nerve is largely derived from water protons and that from orbital fat is largely derived from mobile protons in long chain fatty acids (lipids). When imaging the optic nerve with most sequences the lipid signal is much more intense than the water signal and causes a disproportionate partial volume effect when a small amount of fat is included in a voxel nominally containing optic nerve. Furthermore, movement and data truncation artefacts are exacerbated by the sudden intensity change along the nerve-fat interface, causing lines in the image running parallel to the interface.

A further problem arises because of the chemical shift of lipid protons relative to water protons. When the image is reconstructed no distinction can be made between frequency shifts due to the chemical shift and those due to spatial encoding by the "read gradient". Thus the image of lipid protons is displaced by several pixels relative to the image of water protons. This misregistration of the two images causes a "chemical shift artefact" at the nerve-fat interface which appears as a bright line if the lipid and water images overlap and a dark line if they are separated.

Several methods have been proposed for suppressing lipid signals.

1. Selective saturation of the lipid signal [1].
2. Selective refocussing of the water signal [2].
3. Simplified chemical shift imaging [3, 4].
4. A *S*hort inversion *T*ime *I*nversion *R*ecovery (or STIR) sequence with inversion time selected to nullify the lipid signal [5].

Methods 1 and 2 require good static field homogeneity since it is impossible to distinguish between chemical shifts and frequency shifts induced by the inhomogeneities. In addition, method 1 requires accurate adjustment of RF (radiofrequency) flip angles and good RF transmitter homogeneity and method 2 cannot be adapted for multi-slice data acquisition. Method 3 is also prone to static field inhomogeneity effects and at least doubles imaging time. The fourth (STIR) method, however, is relatively insensitive to static and RF field inhomogeneities.

Lipid suppression alone, however, is insufficient to make the STIR sequence useful. The sequence

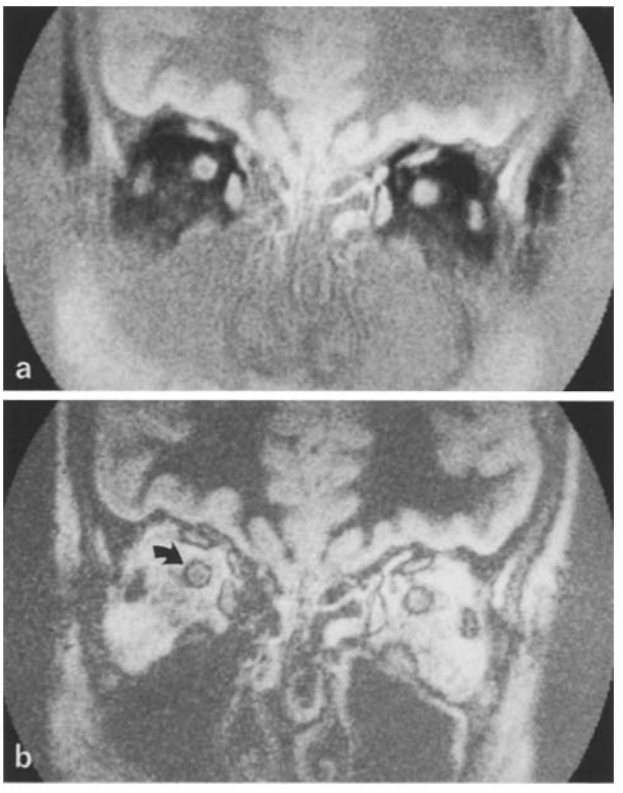

Fig. 1a, b. Cancellation artefact in magnitude reconstruction of IR images. **a** Real reconstruction of $IR_{1560/200/40}$ image. **b** Magnitude reconstruction of same image. *Arrow* indicates artefact

must also be capable of demonstrating pathological changes in the optic nerve i.e. it must provide adequate contrast between normal and abnormal tissues.

We have, therefore investigated the use of STIR sequences for clinical imaging of the optic nerve. We have found that STIR sequences provide adequate suppression of the orbital fat signal and have compared the contrast obtained from STIR sequences with that obtained from conventional (long inversion time) inversion recovery, spin echo and partial saturation sequences with particular reference to the detection of optic neuritis.

The STIR sequence and lipid suppression

The image intensity of a pixel in an inversion recovery (IR) image, I_{IR}, is given by the equation:

$$I_{IR} = G.N.\exp(-T_E/T_2).\{1-2.\exp(-T_I/T_1)+\exp(-T_R/T_1)\} \quad (1)$$

G is a constant expressing system gain; N is the density of mobile protons; T_E is the echo time (assuming a spin echo is used to read out the data); T_I is the inversion time; T_R is the repetition time; T_1 and T_2 are the longitudinal and transverse relaxation times respectively.

It is clear from Equation (1) that the image intensity is negative when $T_I \ll T_1$ and positive when $T_I \gg T_1$. For $T_R \gg T_1$ the null point (the value of T_I for which I_{IR} is zero) is given approximately by

$$T_{Inull} \approx T_1 \cdot \ln 2 \quad (2)$$

At finite values of T_R, T_{Inull} will be shorter than the value given in Equation (2).

A STIR sequence is a Short T_I IR sequence in which the image intensity of most tissues is still negative. STIR sequences can be used to suppress the lipid signal because lipid protons have a uniquely short T_1. Thus if T_I is chosen so that the lipid signal is approximately zero other tissues will have relaxed less than lipid and will still give a substantial negative signal. It is usual, however, to reverse the polarity of the image before display (i.e. multiply all image intensities by -1) since images where tissues are darker than the background are unfamiliar. After the polarity has been reversed most tissues appear light and lipids appears dark in STIR images.

The real part of an IR image is often displayed in preference to the magnitude despite the greater tolerance of field inhomogeneities that magnitude images show. Real IR images are prefered because magnitude images lose the polarity information so that both positive and negative signals appear positive. This effect not only introduces ambiguities into image intensity values [6] but can also cause another artefact (independent of whether there is a chemical shift artefact): a line of zero signal can appear at the interface between regions giving positive and regions giving negative signals, both of which appear bright in the magnitude image [7]. This is illustrated in Figure 1 which gives real (Fig. 1a) and magnitude (Fig. 1b) reconstructions of a coronal IR image ($T_I = 200$ ms) through the optic nerve. The artefactual black ring between the lighter fat and nerve is clearly seen in the magnitude image. In a STIR sequence, however, the only tissue that might give negative signal in a real image is fat. T_I is chosen, however, so that the fat signal is approximately zero and consequently the ring artefact will not be very marked. The STIR sequence therefore has the further advantage over conventional IR sequences that a magnitude reconstruction, with its attendant advantages, can be used with little danger of this artefact.

The chemical shift artefact

The frequency change caused by a chemical shift, k, relative to water protons is $k.f_0$ where f_0 is the water proton Larmor frequency. The pixel bandwidth (i.e.

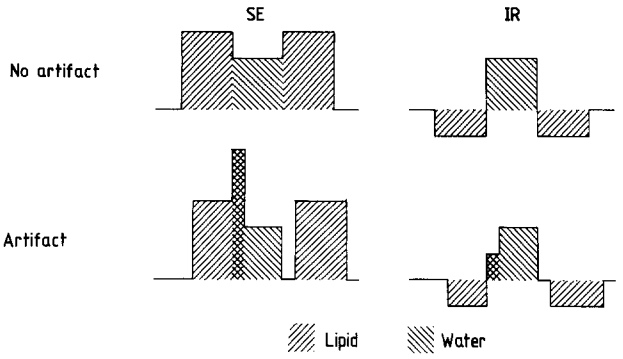

Fig. 2. The chemical shift artefact. The diagrams give the one dimensional profile of image intensity against position for a simple object consisting of a block of water surrounded by fat. Profiles in the abscence of an artefact are given at the top, artefactual profiles are given at the bottom. The effect on a normal sequence with both fat and water giving positive signals (e.g. an SE) is shown on the left. The effect on a sequence where the fat signal is negative relative to the water signal (i.e. an IR) is shown on the right

the change in Larmor frequency caused by the action of the read gradient across the width of a single pixel) is given by f_{bw}/N_{pix} where F_{bw} is the total signal bandwidth and N_{pix} is the number of independent pixels in the direction of the read gradient. Consequently the lipid image is displaced relative to the water image by n pixels where

$$n = N_{pix} \cdot k \cdot f_0 / f_{bw} \tag{3}$$

At 0.5 T (the field strength of our imager) $f_0 = 20$ MHz and $f_{bw} = 10$ kHz for a head image. Thus the lipid image ($k = 3.5$ ppm) will be displaced by about 2 pixels (2 mm) in a 256×256 image.

Figure 2 illustrates the chemical shift artefact that occurs at lipid-water interfaces. The left hand diagrams show the artefact for conventional imaging sequences where both water and lipid signals are positive. At one interface the lipid and water images overlap giving increased signal and at the opposite interface they are separated giving no signal. With IR sequences, however, there may be a lipid signal which is negative relative to the water signal. (With STIR sequences chosen for lipid suppression this signal should be small. With natural variations in relaxtion times, however, suppression is unlikely to be perfect.) If the lipid signal is negative relative to the water signal then the signal at the overlap will be smaller than the pure water signal. In practice this may cause the diameter of the optic nerve to be underestimated although the error introduced by partial volume effects is likely to be much greater. It is probably preferable to select a value of T_I that gives a slightly negative lipid signal since an area of reduced intensity is unlikely to be mistaken for a lesion, which usually appear bright.

Contrast

The contrast in an image is the difference in image intensities between tissues of interest. In STIR sequences pathological tissues with elevated relaxation times give a larger negative signal. After the polarity of the image is reversed lesions appear bright relative to normal tissue.

Contrast, C, can be calculated by subtracting the image intensity of the optic nerve from that of the lesion. Image intensities can be derived by putting the appropriate parameters into Equation (2). Similar values can be obtained for spin echo (SE) and partial saturation (PS) using the standard equations [8].

Since high contrast is of little use if accompanied by high levels of noise, contrast-to-noise ratio (CNR) is a more useful parameter to consider when comparing sequences. For given spatial resolution, number of averages, hardware (e.g. receiver coil) and patient, the noise in an image is fixed and is independent of the sequence used. CNR can be improved, however, by signal averaging. Like signal-to-noise ratio CNR is proportional to the square root of the number of averages:

$$CNR \propto C \cdot \sqrt{N_{av}} \tag{4}$$

where N_{av} is the number of averages. In a fixed total imaging time N_{av} is inversely proportional to T_R. This is not quite the end of the story, however. One slice is usually insufficient to cover the region of interest but there is a practical limit to the number of slices that can be acquired in a multi-slice sequence with a particular value of T_R. If this number of slices is insufficient to cover the volume of tissue to be examined then additional sequences will have to be performed. N_{av} is then related to T_R by the expression:

$$N_{av} \propto 1/N_{seq} \cdot T_R \tag{5}$$

where N_{seq} is the number of times the sequence has to be repeated to cover the volume of interest. Combining Equations (4) and (5) gives an expression for the contrast efficiency of a sequence, D, proportional to CNR per unit imaging time:

$$D = C/\sqrt{N_{seq} \cdot T_R} \tag{6}$$

There are further practical considerations which influence the choice of sequence. First, short sequences have the advantage that total examination time can be reduced or a greater variety of sequences can be performed during an examination. However, if the contrast efficiency of the short T_R sequence is already low it is unlikely that useful images will be obtained without signal averaging. Secondly, the operator may not always choose the sequence with the

Table 1. Relaxation times and relative spin densities. Four normal controls, five MS patients

Tissue	No. of samps.	N[1]		T_1/ms		T_2/ms	
		Range	Mean	Range	Mean	Range	Mean
White matter	9	-	-	370–406	385	73- 92	82
Orbital fat	9	1.5–1.8	1.6	174–270	215	60- 68	63
MS lesion	5	1.0–1.3	1.2	560–785	693	122–281	198

[1] Expressed as fraction of white matter value

highest CNR for the lesion under investigation since other regions in the resultant image may not then be displayed adequately. Nevertheless, Equation (6) does provide an objective method of comparing sequences.

Materials and methods

Relaxation times and spin densities were obtained from three-point measurements [9] on four normal volunteers and five patients with clinically definite MS diagnosed according to the Washington criteria [10]. Measurements were made on orbital fat, frontal white matter and MS lesions. Ideally the NMR characteristics of the optic nerve itself would be used to calculate optimum sequences. However, no attempt was made to measure the relaxation times of the optic nerve or lesions within it directly since partial volume effects introduce considerable imprecision due to the small size of the nerve. Instead it was assumed that the optic nerve would have similar relaxation times and proton density to cerebral white matter. It was also assumed that optic nerve lesions in MS would have similar properties to MS lesions in the white matter of the cerebral hemispheres.

Spin densities were expressed as a percentage of the frontal white matter value since there are day-to-day fluctuations in image intensity which prevent precise absolute measurements.

The values of relaxation times and proton densities were used in conjuction with relaxation times measured from presumed demyelinating lesions in the brain stem [11] to give parameters for a "chronic" and an "acute" MS lesion.

The measured orbital fat T_1's were used to predict a value of T_{Inull} by Equation (2). This was then checked by performing IR scans with $T_I = 0$, 50, 100, 150 and 200 ms and finding T_{Inull} from plots of the relaxation curves. The proton densities and relaxation times were used to estimate how much residual fat signal might be expected as a result of the natural variation in these parameters.

Relaxation times and proton densities were used to obtain estimations of D for STIR, IR, SE and PS sequences. D values for the "acute" and the "chronic" lesion relative to white matter were considered.

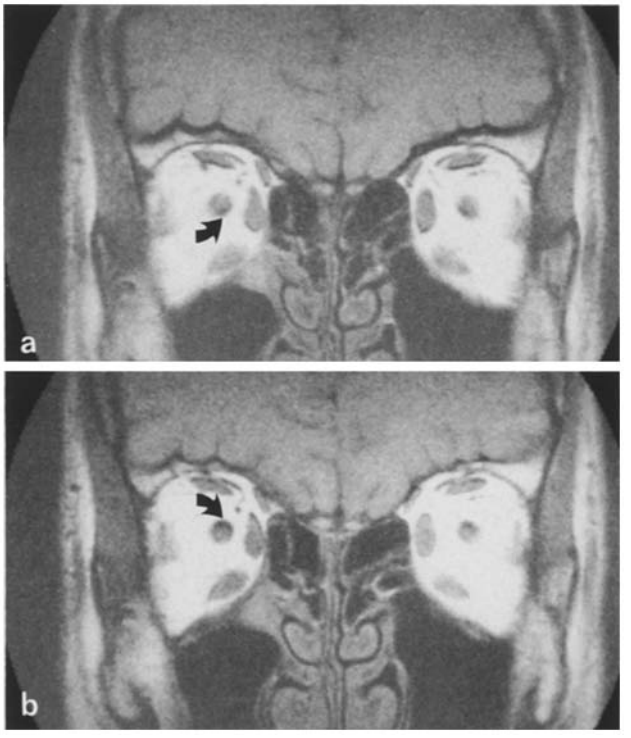

Fig. 3a, b. Coronal $SE_{500/40}$ image illustrating the chemical shift artefact. In Figure 2a a black line *(arrow)* appears at the bottom of the optic nerve and orbital muscles (the bright line at the top is difficult to distinguish from surrounding fat with this display window). In Figure 2b the polarity of the read gradient has been reversed and the black line now appears at the top

The effect that variations in the imaging parameters have on D values were studied graphically and a "standard" STIR sequence was compared with the optimum IR, SE and PS sequences (obtained graphically). We took an $IR_{1560/150/40}$ as our "standard" STIR sequence for the following reasons: 1560 ms is the minimum T_R for this STIR sequence with 6 slices; 150 ms is slightly longer than T_{Inull} but a longer value is probably preferable for the reason given above; 40 ms is the minimum T_E available with 15 cm field of view scans on our imager.

All imaging was performed on a Picker 0.5 T imager. Unless otherwise stated all the images illustrated are 256×256 pixels, two signal averages and 15 cm diameter field of view. They are obtained from six contiguous slice multi-slice sets with 5 mm slice

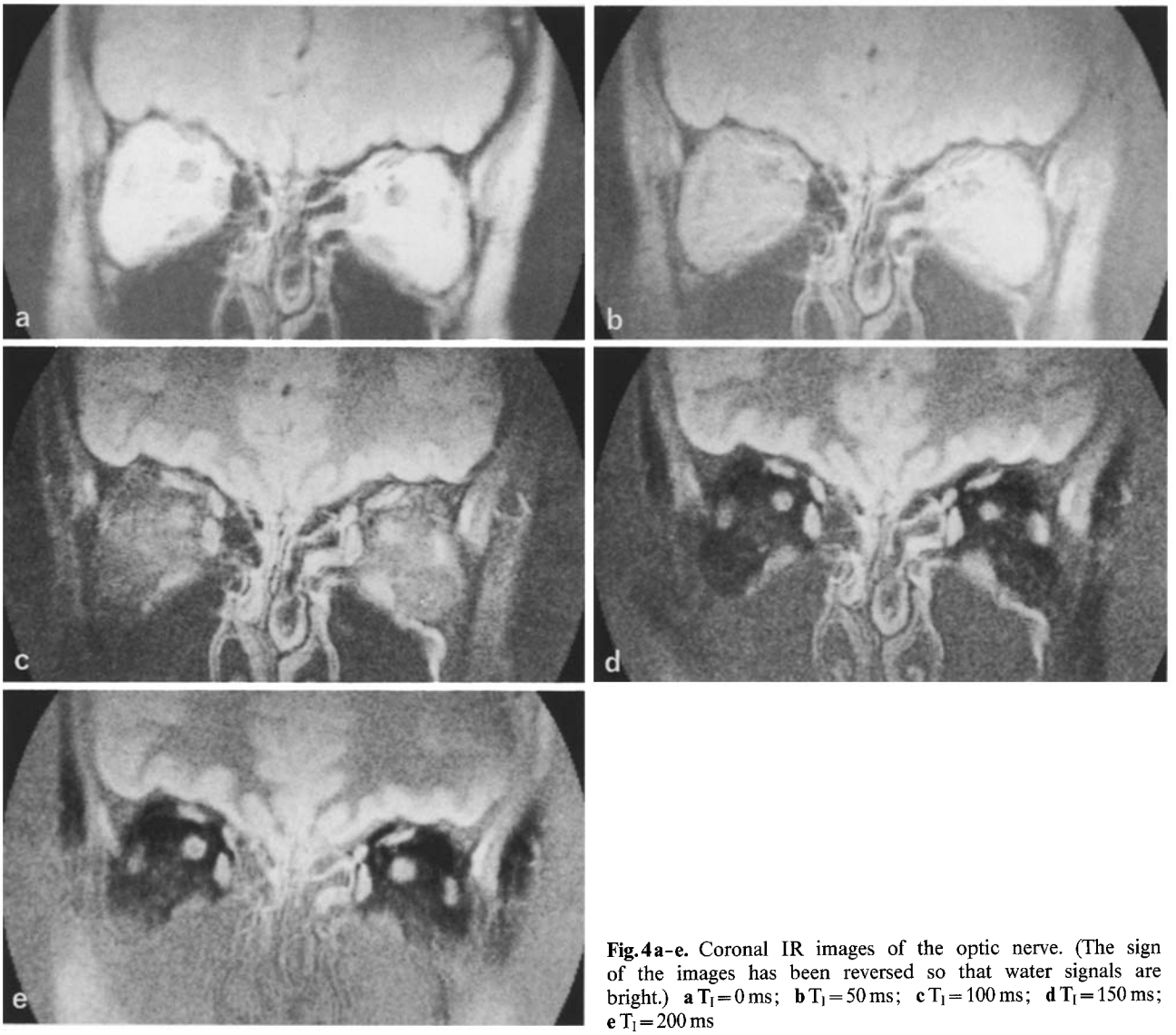

Fig. 4a–e. Coronal IR images of the optic nerve. (The sign of the images has been reversed so that water signals are bright.) **a** $T_I = 0$ ms; **b** $T_I = 50$ ms; **c** $T_I = 100$ ms; **d** $T_I = 150$ ms; **e** $T_I = 200$ ms

width. Six coronal 5 mm slices are sufficient to image the intra-orbital portion of the optic nerve. In all cases the direction of the read gradient (and hence the chemical shift artefact) is vertical.

The nomenclature used to describe the sequences is $SE_{TR/TE}$ for SE sequences and $IR_{TR/TI/TE}$ for IR sequences.

Results

The problems involved in imaging the optic nerve are illustrated in Fig. 3 which gives two $SE_{500/40}$ images through the optic nerve. The polarity of the read gradient was opposite in Fig. 3a and b and consequently the direction of the chemical shift misregistration was reversed between the two images.

Spin densities and relaxation times

Measured relaxation times and spin densities are given in Table 1. Relaxation times of cerebral white matter are comparable with those obtained previously [9] and values for the cerebral lesions are comparable with previously published values for chronic brain stem lesions [11]. The T_1 of acute lesions, however, can be as long as 1200 ms, probably due to greater water content [12]. It seems likely that in the optic nerve, too, the highest values of proton density will be associated with acute lesions and less high values with chronic lesions.

Lipid suppression

The suppression of the lipid signal depends on T_I being chosen to correspond to T_{Inull} in Equation (3).

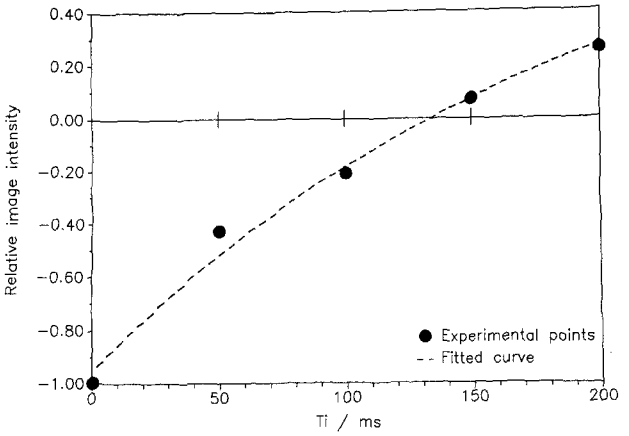

Fig. 5. T_1 decay curve for orbital fat obtained from the images in Figure 3

The T_1 values for orbital fat in Table 1 give a range of T_{Inull} (using Equation (3)) from 120 to 190 with a mean of 150 ms. Figure 4 shows the optic nerve in five coronal IR images ($T_R = 1560$ ms, $T_I = 0$, 50, 100, 150 and 200 ms). The polarity of these images is reversed so that more negative signal (e.g. the nerve) appears white and less negative and positive signals (i.e. fat) appear black. T_I values of 100 ms and 150 ms both give very good fat suppression with no obvious chemical shift artefact.

Figure 5 gives a plot of image intensity against T_I for the orbital fat. $T_{Inull} = 135$ ms, corresponding to a T_1 of 195 ms. (At this T_1 the approximation of Equation (3) will be good.) In general it was found that $T_I = 150$ ms was rather longer than the true value of T_{Inull}. This suggests that the measurements underestimate T_1. This is likely to be due to bi-exponential T_1 relaxation of fat [13]. Our two point measurement of T_1 will tend to emphasize the longer, aqueous component of relaxation because of the long T_I of the IR sequence used in the calculation.

Contrast

The proton densities and relaxation times used to calculate contrast efficiency for the "acute" lesion (D_{acute}) and "chronic" lesion ($D_{chronic}$) are given in Table 2.

Fig. 6 gives plots of D_{acute} and $D_{chronic}$ against the different IR parameters as they vary from those of the standard STIR sequence. STIR contrast could be improved, particularly for acute lesions, by increasing T_R and T_I. However, the improvement at longer T_R's is small and increasing T_I would decrease lipid suppression.

Inspection of Fig. 6 indicates that the IR sequence cannot be optimised for D_{acute} and $D_{chronic}$ simultaneously. As one would expect D_{acute} is much larger than $D_{chronic}$ so it is probably preferable to fa-

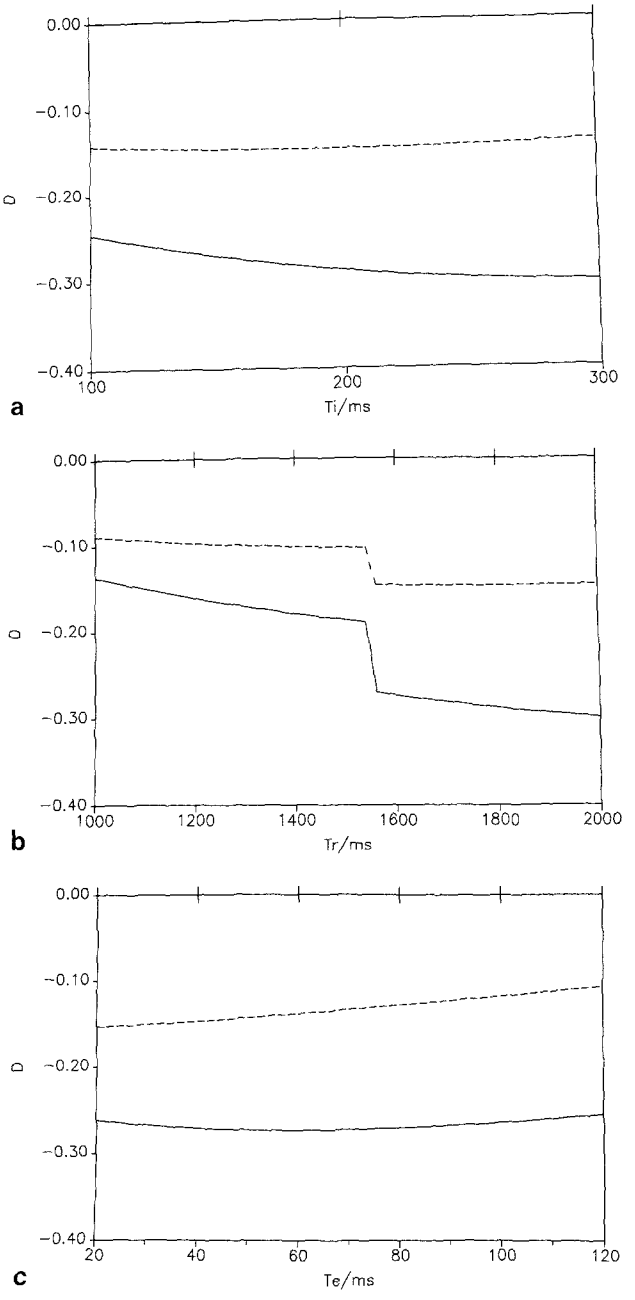

Fig. 6a–c. Variation of D_{acute} (solid line) and $D_{chronic}$ (dashed line) with variations in IR parameters for a six slice multi-slice scan. **a** D vs. T_I. $T_R = 1560$ ms, $T_E = 40$ ms. **b** D vs. T_R. $T_I = 150$ ms, $T_E = 40$ ms. **c** D vs. T_E. $T_R = 1560$ ms, $T_I = 150$ ms. The discontinuity in b) occurs because the sequence has to be repeated to give six slices at short T_R's (i.e. $N_{seq} = 2$ in Equation (6))

Table 2. Relaxation times and relative spin densities used in comparisons of contrast

Tissue	N[1]	T_1/ms	T_2/ms
White matter	1	385	82
Acute MS lesion	1.3	1200	250
Chronic MS lesion	1.1	600	130

[1] Expressed as fraction of white matter value

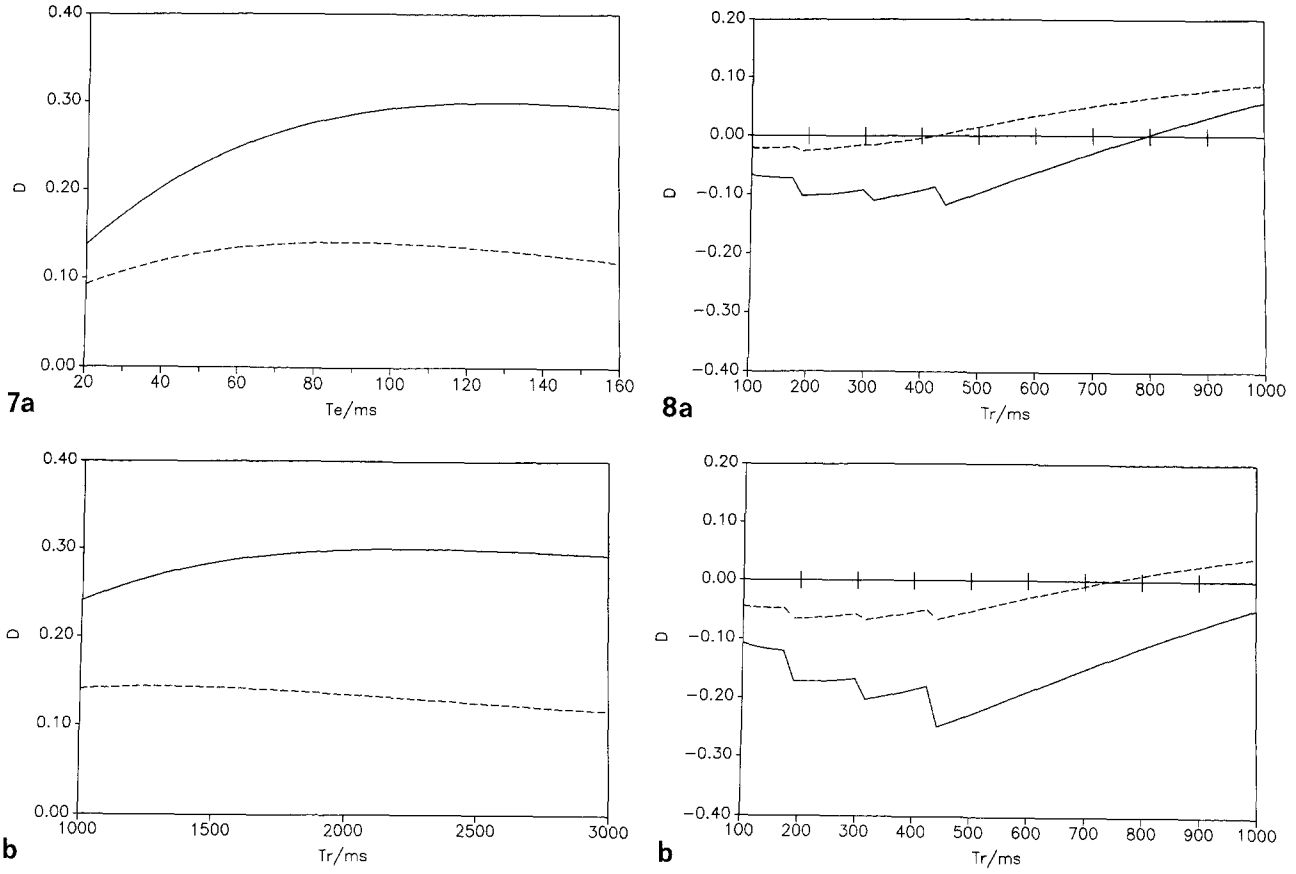

Fig. 7 a, b. Variation of D_{acute} (solid line) and $D_{chronic}$(dashed line) with variations in SE parameters for a six slice multi-slice scan. **a** D vs. T_E. $T_R = 2000$ ms. **b** D vs. T_R. $T_E = 120$ ms

Fig. 8 a, b. Variation of D_{acute} (solid line) and $D_{chronic}$ (dashed line) with variations in PS parameters for a six slice multi-slice scan. **a** D vs. T_R. $T_E = 40$ ms. **b** D vs. T_R. $T_E = 20$ ms. The discontinuities are due to the number of times the sequence has to be repeated to give six slices

Table 3. Contrast efficiency of STIR and optimum IR, SE and PS sequences

	D_{acute}	$D_{chronic}$
$IR_{1560/150/40}$ (STIR)	−0.271	−0.174
$IR_{2000/250/40}$	−0.324	−0.145
$SE_{2000/120}$	0.299	0.135
$SE_{450/20}$ (PS)	−0.246	−0.063

vour a sequence which is more sensitive to chronic lesions. A suitable compromise might be an $IR_{2000/250/40}$.

Fig. 7 gives plots of D_{acute} and $D_{chronic}$ against SE parameters. Again there is no single optimum but an $SE_{2000/120}$ would be a suitable compromise.

Fig. 8 a is a plot of D_{acute} and $D_{chronic}$ vs. T_R for the SE sequence ($T_E = 40$ ms) used as a PS sequence to give T_1 contrast. The calculated contrast is much inferior to that of the IR and SE sequences because differences in N and T_2 tend to cancel out T_1 contrast. Reducing T_E to 20 ms would give much better values of D since less T_2 decay will have occurred (Figure 8 b). However, this would probably have to be achieved by decreasing the data collection interval and the consequent increase in signal bandwidth will increase noise. Nevertheless, for comparison purposes we will consider the $SE_{450/20}$ as the optimum PS sequence.

Table 3 gives values of D_{acute} and $D_{chronic}$ for the standard STIR sequence and the optimum IR, SE and PS sequences. The standard STIR sequence gives 84% of the best D_{acute} value (which comes from the $IR_{2000/250/40}$) and the best $D_{chronic}$ (120% of the $SE_{2000/120}$). It would be possible to improve $D_{chronic}$ for the SE sequence (e.g. by an $SE_{1300/80}$) but the STIR sequence would still be comparable. Even reducing T_I from 150 ms so that it was closer to T_{Inull}, which would reduce contrast, would still leave it comparable with the other sequences.

Discussion

Suppression of the fat signal is unlikely to be perfect due to variations in relaxation time between individuals. The range of T_1 values in Table 1 could give a range of orbital fat signals between about −8% and +8% of the mean white matter signal in an

$IR_{1560/150/40}$ sequence. The proton density values of fat, however, seem rather high (possibly due to underestimates of white matter proton density caused by neglecting bi-exponential T_2 relaxation of white matter) so that these estimates of the residual fat signal may be too pessimistic.

In predicting values for T_{Inull} appropriate for suppressing the lipid signal and the chemical shift artefact we have assumed that in orbital fat only lipid gives a signal and that this signal has a mono-exponential T_1. In fact a significant fraction of the signal will be derived from water protons so T_1 will be bi-exponential. This has two consequences. Firstly, as already stated, T_{Inull} is overestimated by two point measurements of T_1. Secondly, even at the true null point (where the *total* signal is zero) the more rapidly relaxing lipid component will have already passed the zero point. As it is only this component that gives the chemical shift artefact we might fear an artefact even when T_I is chosen so that the total fat signal is zero. But again, because this signal component is negative relative to the nerve signal it will only lead to an apparent narrowing of the nerve. The estimate of the range of residual fat signals above is likely to be realistic but the mean will be negative rather than zero. In practice, at a T_I of 150 ms we have never been aware of any remaining chemical shift artefact.

It is generally the case that pathological change results in increased water content and elevation of the relaxation times. In PS and SE sequences increases in T_1 and increases in proton density and T_2 produce contrast changes which oppose one another. In conventional IR sequences increases in T_2 and increases in proton density and T_1 produce conflicting contrast changes. STIR sequences are unique in that an increase in any of the parameters increases contrast. Consequently, our finding that STIR contrast compares favourably with that of other sequences is not surprising. Furthermore, STIR contrast is relatively insensitive to changes in the timing parameters (Figure 6) when compared with the sensitivity of SE and PS sequences to changes in T_E and T_R respectively. STIR contrast is therefore relatively unambiguous - a lesion will produce a bright spot regardless of timing parameters or the relative elevation of T_1 and T_2.

In view of the good contrast achieved with STIR sequences over a wide range of different parameters (of the "acute" and "chronic" lesions) it will probably be a good sequence for imaging any pathology of the optic nerve. Since using this sequence we have been able to detect lesions in the optic nerve in 10/14 patients with acute unilateral optic neuritis [14]. Furthermore, its robustness may make it a good sequence for imaging any unknown pathology even where lipid suppression is not required.

Acknowledgements. The NMR imaging research program is supported by generous grants from the Multiple Sclerosis Society of Great Britain and Northern Ireland and the Medical Research Council. We would also like to thank all other members of the NMR/MS group.

References

1. Haase A, Frahm J, Hanicke W, Matthaei D (1985) ^{1}H NMR chemical shift selective (CHESS) imaging. Phys Med Biol 30: 341-344
2. Joseph PM (1985) A spin echo chemical shift MR imaging technique. J Comput Assist Tomogr 9: 651-658
3. Dixon WT (1984) Simple proton spectroscopic imaging. Radiology 153: 189-194
4. Sepponen RE, Sipponen JT, Tanttu JI (1984) A method for chemical shift imaging: demonstration of bone marrow involvement with proton chemical shift imaging. J Comput Assist Tomogr 8: 585-587
5. Bydder GM, Young IR (1985) MR imaging: clinical use of the inversion recovery sequence. J Comput Assist Tomogr 9: 659-674
6. Young IR, Bailes DR, Bydder GM (1985) Apparent changes of appearance of inversion-recovery images. Magn Reson Med 2: 81-85
7. Hearshen D, Ellis J, Carson P, Shreve P, Aisen A (1984) Boundary effects from phase cancellation in inversion recovery images. Book of Abstracts, 3rd Annual Meeting, Society of Magnetic Resonance in Medicine, New York, p 310. Society of Magnetic Resonance in Medicine, Berkeley
8. Ortendahl DA, Hylton N, Kaufman L, Watts JC, Crooks LE, Mills CM, Stark DD (1984) Analytical tools for magnetic resonance imaging. Radiology 153: 479-488
9. Johnson G, Ormerod IEC, Barnes D, Tofts PS, MacManus D (1986) Accuracy and precision in the measurement of relaxation times in NMR imaging. Brit J Radiol (In press)
10. Poser CM, Paty DW, Scheinberg L, McDonald WI, Davis FA, Ebers GC, Johnson KP, Sibley WA, Silberberg DH, Tourtellotte WW (1983) New diagnostic criteria for the clinical diagnosis of multiple sclerosis: Guidelines for research protocols. Ann Neurol 13: 227-231
11. Ormerod IEC, Bronstein A, Rudge P, Johnson G, MacManus D, Barratt H, Halliday AM, du Boulay EPGH, Kendall BE, Moseley IF, Jones SJ, Kriss A, Perringer E (1986) Nuclear magnetic resonance imaging of the brain stem. J Neurol Neurosurg and Psychiatry 49: 737-743
12. Tourtellotte WW, Parker JA (1968) Some spaces and barriers in postmortem multiple sclerosis. Lajtha A, Ford DH (eds) Brain Barrier Systems, Progress in Brain Research 29, 493-525. Amsterdam: Elsevier 1968
13. Bakker CJG, Vriend J (1984) Multi-exponential water proton spin-lattice relaxation in biological tissues and its implications for quantitative NMR imaging. Phys Med Biol 29: 509-518
14. Miller D, Johnson G, McDonald WI, MacManus D, du Boulay EPGH, Kendall BE, Moseley IF (1986) Detection of optic nerve lesions in optic neuritis with magnetic resonance imaging. Lancet 28: 1492

Received: 5 October 1986

Dr. G. Johnson
NMR Unit
Institute of Neurology
Queen Square
London WC1N 3BG
England